# Optimum Melting Temperature and Latent-Heat Contribution of a PCM Layer in Multilayer Walls for Mediterranean, Semi-Arid and Hot Desert Climates

**[1]Belkacem N., [2]Missoum M., [1]Benchamma S.**
[1] Hassiba Benbouali University of Chlef, Chlef, Algeria
[2]University of Tipaza, Tipaza, Algeria

***Abstract***. The main objectives of the paper are to determine, for three climatic zones (Mediterranean coast, semi-arid High Plateau and hot desert), the optimum melting temperature of a PCM layer in a wall for each position and orientation, and, as a new contribution, to separate the benefit of the latent heat from that of the added layer. These objectives were achieved with an enthalpy model verified against the Stefan solution (within 0.2 %), in a periodic regime, for a typical and a heat-wave day of one site per zone. Three PCMs melting within the temperature range of the wall were compared, RT-27 (28 °C) was retained, and its melting temperature was varied from 18 to 44 °C. RT-27 lowered the maximum internal surface temperature by 1.3 °C (median); the latent heat accounted for only 0.1 to 0.5 °C at the optimum melting temperature (20 % of the reduction, median); this optimum, close to the mean daily temperature at the layer, was 28 to 30 °C (walls) and 32 °C (roof) between the bricks on the coast and the High Plateau, and 32 to 35 °C and 38 °C in the Sahara; polystyrene insulation of equal thickness lowered the temperature more than the PCM. The significance is that, on thermal grounds, a PCM layer does not replace insulation, because most of its benefit comes from the added layer, and that its melting temperature should be chosen from the mean daily temperature at the layer, not set to a standard value.
***Keywords*:** phase change material (PCM), heat transfer, numerical simulation, multilayer wall.

**DOI: https://doi.org/10.52254/1857-0070.2026.4-72.16**
**UDC: 697.1:536.2**

**Temperatura optimă de topire și contribuția căldurii latente a unui strat de material cu schimbare de fază (PCM) în pereți multistrat, pentru climate mediteraneene, semiaride și de deșert cald**

**[1]Belkacem N., [2]Missoum M., [1]Benciamma S.**
[1]Universitatea Hassiba Benbouali din Chlef, Chlef, Algeria
[2]Universitea din Tipaza, Chlef, Algeria

***Rezumat***. Obiectivele principale sunt determinarea, pentru trei zone climatice (coasta mediteraneană, platourile înalte semiaride și deșertul cald), a temperaturii optime de topire a unui strat de material cu schimbare de fază (PCM) integrat într-un perete de clădire, în funcție de poziția și orientarea acestuia. O contribuție nouă a lucrării constă în separarea beneficiului adus de căldura latentă de cel oferit de simpla prezență a stratului adăugat. Aceste obiective au fost atinse utilizând un model entalpic unidimensional, verificat prin comparație cu soluția analitică Stefan (cu o eroare de 0.2%), în regim periodic, pentru o zi tipică și o zi de caniculă dintr-o locație pentru fiecare zonă. Au fost comparate trei PCM-uri a căror temperatură de topire se află în intervalul atins în perete; RT-27 (28 °C) a fost reținut, iar temperatura sa de topire a fost variată între 18 și 44 °C. RT-27 a redus temperatura maximă a suprafeței interioare cu 1.3 °C (mediană); aportul căldurii latente a fost de doar 0.1–0.5 °C la temperatura optimă de topire (mediană de 20% din reducere); această temperatură optimă, apropiată de temperatura medie zilnică de la poziția stratului, a fost de 28–30 °C pentru pereți și 32 °C pentru acoperiș, între cărămizi, în zonele de coastă și pe platourile înalte, respectiv 32–35 °C și 38 °C în Sahara; izolația din polistiren de aceeași grosime a redus temperatura mai mult decât PCM-ul. Semnificația constă în faptul că, din punct de vedere termic, un strat de PCM nu înlocuiește izolația, deoarece cea mai mare parte a beneficiului provine din stratul adăugat, și că temperatura sa de topire trebuie aleasă pe baza temperaturii medii zilnice de la poziția stratului, nu fixată la o valoare standard.
***Cuvinte-cheie***: material cu schimbare de fază (PCM), transfer termic, simulare numerică, perete multistrat.

©Belkacem N., Missoum M., Benchamma S.
2026

**Оптимальная температура плавления и вклад скрытой теплоты фазового перехода в многослойных ограждающих конструкциях для средиземноморского, полузасушливого и жаркого пустынного климата**

**[1]Белкасем Н., [2]Миссум М., [1]Беншамма С**.
[1] Университет Хассиба Бенбуали в Шлефе, г. Шлеф, Алжир
[2]Университет Типазы, г. Шлеф, Алжир

***Аннотация***. Основная цель работы — определение оптимальной температуры плавления материала с фазовым переходом (МФП) в составе многослойной строительной конструкции для различных вариантов ее расположения и ориентации в трех климатических зонах (средиземноморское побережье, полузасушливые Высокие плато и жаркие пустыни). В качестве нового научного вклада предложен подход, позволяющий разделить эффект от использования скрытой теплоты фазового перехода и эффект от самого факта добавления дополнительного слоя в конструкцию. Для решения поставленных задач использовалась одномерная энтальпийная модель, верифицированная путем сопоставления с аналитическим решением задачи Стефана (погрешность в пределах 0.2 %); расчеты выполнялись в периодическом режиме для типичного дня и дня аномальной жары по одному пункту в каждой зоне. Сравнивались три МФП, температура плавления которых лежит в диапазоне температур стены; был выбран RT-27 (28 °C), и его температура плавления варьировалась от 18 до 44 °C. RT-27 снижает максимальную температуру внутренней поверхности на 1.3 °C (медиана); вклад скрытой теплоты при оптимальной температуре плавления составляет лишь 0.1–0.5 °C (медиана 20 % от снижения); эта оптимальная температура, близкая к средней суточной температуре в месте расположения слоя, для слоя между кирпичными слоями составила 28–30 °C для стен и 32 °C для кровли на побережье и на Высоких плато и 32–35 °C и 38 °C в Сахаре; изоляция из пенополистирола той же толщины снижает температуру сильнее, чем МФП. Значимость заключается в том, что с тепловой точки зрения слой МФП не заменяет теплоизоляцию, поскольку основной эффект дает сам добавленный слой, и что его температуру плавления следует выбирать по средней суточной температуре в месте расположения слоя, а не принимать стандартной.

***Ключевые слова***: материал с фазовым переходом (МФП), теплопередача, численное моделирование, многослойная ограждающая конструкция.

## INTRODUCTION

Through combining initiatives and the acquisition of knowledge, Algeria is engaged to decrease energy use in buildings and enhance energy efficiency within the building sector. However, rapid urbanization and low-cost construction mean that most buildings are not climate-adaptive, built without thermal insulation considerations, and commonly use double hollow brick cavity (DHB) [1]. Beyond insulation, passive solutions such as the incorporation of phase change materials (PCM) have shown a positive impact in controlling thermal loads and achieving energy savings [2].

PCM is a kind of material that can absorb and release large amounts of latent heat during melting and solidification processes, thereby reducing heating and cooling loads, and maintaining an acceptable thermal comfort, with an enhanced ability to store thermal energy compared to conventional materials [3].

PCMs reduce indoor temperature fluctuations [4], and their efficiency depends on their type, thickness, location in the building envelope and local climate [5].

Numerical models have been developed to predict how the integration of PCM affects the thermal performance of buildings [6]. Khan et al. [7] and Lajimi et al. [8] found that a PCM layer close to the exterior reduces heat transfer more, whereas Nateghi et al. [9] and Liu et al. [10] found the inner part of the wall more effective; Kishore et al. [11] and Zhu et al. [12] showed that the optimal location depends on the climate.

The thickness of the layer is as important as its position [13, 14]: a larger thickness reduces heating and cooling energy [15, 16], up to a critical value [17]. Dashtaki et al. [18] and Guermat et al. [19] found that a melting temperature close to indoor conditions gives the largest savings, and the optimal phase-transition temperature depends on the climate and the season [20–22]. A CenoPCM wall regulates the indoor surface temperature better [23], and an optimal incorporation balances thermal and mechanical performance, with climate-dependent benefits [24, 25].

PCM wallboards and panels are the most common way of integrating PCM into buildings, owing to their easy installation and low cost.

These studies show that the position, the thickness and the type of the PCM all matter, but most of them change one parameter at a time, each with its own wall, climate and boundary conditions, so the results cannot be compared directly (best position: exterior in [7, 8], interior in [9, 10],

climate-dependent in [11, 12]). Wall orientation, which fixes the solar load and therefore the melting and solidification cycle, is rarely combined with position and type, hybrid walls [26] and PCM geometry [27] are different questions, and only a few studies address Algerian conditions [1, 19]. Optimisation of the melting temperature has been reported for Algerian climates at building level [28] but, to our knowledge, not at wall level for each position and orientation, nor with the latent heat separated from the effect of the added layer.

The novelty of this work is threefold. First, the benefit of a PCM layer in a wall is split, with the same model, into the part due to the added layer and the part due to the latent heat, which is rarely done. Second, the optimum melting temperature is determined for each position of the layer and for each orientation of the wall (roof, south, east, west and north walls), and not for a single wall. Third, it is determined with the same method for three contrasted climatic zones, the Mediterranean coast, the semi-arid High Plateau and the hot desert, so that the zones can be compared.

The objectives of the article are:

(1) to quantify the effect of a PCM layer on the internal surface temperature and on the heat flux of a brick wall;

(2) to find the best position of the layer and to determine the influence of the orientation of the wall;

(3) to compare three PCMs whose melting temperature lies in the range reached in the wall and to select the reference PCM;

(4) to separate the benefit of the latent heat from that of the added layer, and to determine the optimum melting temperature for each position, orientation and climatic zone, to compare it with the mean daily temperature of the wall, in order to give selection criteria for PCM wall panels in comparable climates.

To reach these objectives, one enthalpy-based finite-difference model, with the same wall, boundary conditions and numerical scheme, is used in a periodic regime, on a typical and a heat-wave day of one site per climatic zone: the effect of the PCM, its position, the wall orientation and three PCMs are compared first, then the melting temperature is varied continuously and compared with the mean daily temperature of the wall.

## I. THEORETICAL FOUNDATION

### *A. Energy that a PCM layer can store*

A PCM layer of thickness e and density ρ stores latent heat only while it melts, and the maximum energy per unit area that it can absorb in this way is

$$E_{\max} = \rho . L_f . e \qquad (T1)$$

that is 6.4 MJ/m² (1.8 kWh/m²) for a 0.05 m layer of RT-27. This energy is used only if the melting temperature lies within the range of temperature that the layer reaches during the day,

$$T_{\min} < T_m < T_{\max} \qquad (T2)$$

where Tmin and Tmax are the daily minimum and maximum temperatures of the layer. If Tm < Tmin the PCM stays liquid and acts only as a sensible layer, and if Tm > Tmax it stays solid. The range [Tmin, Tmax] is fixed by the position of the layer in the wall, by the orientation of the wall, which fixes the solar load, and by the climate. The melting temperature is therefore the design variable that links the PCM to a climatic zone.

### *B. Separation of the added layer and of the latent heat*

A PCM layer changes the wall in two ways: it adds a layer with its own thermal mass and resistance, and it adds the latent heat. To separate the two effects, three walls with the same geometry and boundary conditions are compared: the reference wall without PCM (index 0), the wall with the layer whose latent heat is set to zero (Lf = 0, index L), which keeps the density, the specific heat and the conductivity of the PCM, and the wall with the PCM (index P). For an indicator Y (the maximum internal surface temperature Tsi,max, or the daily heat gain), the effect of the added layer and the effect of the latent heat are

$$\Delta Y_{layer} = Y_0 - Y_L , \Delta Y_{lat} = Y_L - Y_P \qquad (T3)$$

their sum is the total effect,

$$\Delta Y_{tot} = Y_0 - Y_P = \Delta Y_{layer} + \Delta Y_{lat} \qquad (T4)$$

and the share of the latent heat in the total effect is

$$\varphi = \Delta Y_{lat} / \Delta Y_{tot} \qquad (T5)$$

Because the layer L and the PCM have the same sensible properties, ΔYlat is entirely due to the phase change. It is zero when the PCM is completely liquid or completely solid during the whole day, which is the case of the PCMs melting below the temperatures of the wall and of RT-27 between the bricks in the Sahara.

*C. Optimum melting temperature*

For a position p, a surface o (roof, south, east, west or north wall) and a zone z, K design days k are considered (here K = 2: a typical sunny day and a heat-wave day). The loss of a melting temperature Tm on day k is the excess of the maximum internal surface temperature over its lowest value obtained when Tm is varied,

$$r_k(T_m) = T_{si,\max,k}(T_m) - \min T_{si,\max,k}(T') \qquad (T6)$$

and the optimum melting temperature is the one with the lowest mean loss,

$$T_m^* = \arg\min(1/K)\sum r_k(T_m) \qquad (T7)$$

The same mean loss, evaluated for a commercial PCM (Tm = 28 °C for RT-27), measures what is lost by not choosing the melting temperature of the zone. The indicators are computed with the model of Sections II and III, which is applied in Sections IV and V to the three climatic zones.

## II. PROPOSED MODEL

Exterior walls are the largest surface area of a building in contact with the outside environment. They are constantly exposed to variable weather conditions and are a primary source of heat losses in winter and heat gains in summer. Therefore, they have gained special attention for the integration of PCMs in building walls to control indoor temperature and reduce energy consumption while balancing the greenhouse effect [24].

Figure 1 shows the vertical cross-sectional area of the walls considered in this study. Figure 1 (a) depicts the typical wall assembly (no PCM), presenting a typical wall of a building in these climates, consisting of a single 30 cm brick [29]. PCM can be integrated into the wall in various ways, and each of these methods has certain advantages and disadvantages.

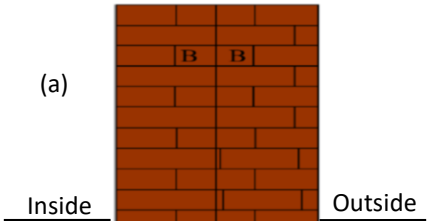



**Fig.1. Vertical cross-section of the: (a) typical brick wall without PCM integration, (b) PCM integrated wall containing a layer of PCM between brick layers.**

Obtaining uniform PCM distribution in the building materials is usually difficult [3]. Here, a PCM layer is sandwiched inside the wall between two bricks, as shown in Figure 1 (b).

Table 1 and table 2 depict the material properties of the different components of the wall considered in this study [29, 30].

*Table 1*

Brick properties

| Brick | |
|---|---|
| Dimension (m) | 0.3×0.2×0.15 |
| Specific heat C ($\frac{J}{kg.K}$) | 840 |
| Density ρ ($\frac{kg}{m^3}$) | 1800 |
| Thermal conductivity λ ($\frac{W}{m.K}$) | 0.72 |

*Table 2*

PCM properties (Rubitherm RT-27)

| PCM RT-27 | |
|---|---|
| Class | Organic |
| Type | Paraffin |
| Melting temperature Tm (°C) | 28 |
| Latent heat of fusion Lf ($\frac{kJ}{kg}$) | 147 |
| Specific heat C ($\frac{J}{kg.K}$) | 2000 |
| Density ρ ($\frac{kg}{m^3}$) | 870 |
| Thermal conductivity λ ($\frac{W}{m.K}$) | 0.2 |

This selected PCM is widely utilized in building applications, easily available, and its thermophysical properties are well known. Organic PCMs (paraffins) are safe and recyclable,

whereas inorganic PCMs (salt hydrates) have a high storage capacity, good conductivity and low cost [31]. RT-27 was chosen a priori as a widely used paraffin whose melting temperature (28 °C) is close to the comfort temperature and above the initial temperature of the wall, so that it melts during the day[32]; the comparison of three PCMs (Section V.D) then confirms that it gives the largest reduction. The properties of Table 2 are the manufacturer values; other sources report a melting range of 24.5 to 30 °C and a latent heat of 147 to 189 kJ/kg for RT-27, so the effect of this variability is discussed with the limitations.

## III. DISCRETIZATION AND MATHEMATICAL MODELING

### *A. Physical model*

The PCM integrated wall considered in this study is a multilayer wall with exterior and interior wallboards, each having thickness of 0.15 m, while the PCM layer has a thickness of 0.05 m, resulting in total wall thickness 0.35 m. As shown in figure 02, yellow nodes (n for indoor and o for outdoor) represent boundary nodes of the wall, capturing convection and radiation boundary conditions. Red nodes represent interior solid nodes, indicating the temperature profile and ther mal storage inside the brick material. Green nodes, situated at the interface between the brick layer and PCM, denote the thermal contact between the two distinct materials. Blue node denotes monitoring of heat transfer in the PCM core.

**Fig 2. Discretization of a PCM-integrated wall.**

### *B. Boundary conditions*

The outside wall surface is exposed to a convective heat transfer , characterized by ($h_c$, $T_{\infty,o}$), a radiative heat transfer $q_{c,o}$ characterized by ($h_{r,o}$, $T_{sky}$), in addition to a fraction of the incident solar energy $I$ [33, 34]. The total heat exchange at this boundary is expressed by the following relation:

$$-\lambda \frac{\partial T}{\partial x}\bigg|_{x=0} = \alpha \times I + h_{c,o} \times \left(T_o - T_{x=0}\right) + h_{r,o} \times \left(T_{sky} - T_{x=0}\right) \quad (1)$$

Where, the apparent sky temperature is calculated based on ($T_o$) using the following relation:

$$T_{sky} = 0.0552 T_o^{1.5} \quad (2)$$

And, the radiative heat transfer coefficient on the outside of the multi-layer wall is calculated using the following expression:

$$h_{r,o} = \varepsilon\sigma\left(T_{sky}^2 + T_{x=0}^2\right)\left(T_{sky} + T_{x=0}\right) \quad (3)$$

The inside wall surface is exposed to a convective heat transfer, characterized by ($h_{c,i}$, $T_{\infty,i}$) and is expressed by the following relation:

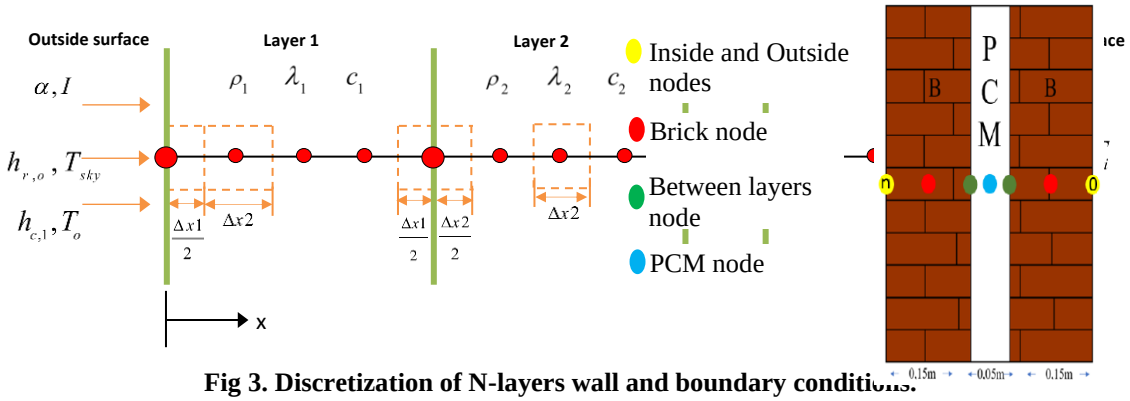



**Fig 3. Discretization of N-layers wall and boundary conditions.**

$$-\lambda \left.\frac{\partial T}{\partial x}\right|_{x=L} = h_{c,i} \times \left(T_{x=L} - T_i\right) \quad (4)$$

*C. Mathematical model*

To predict the thermal behaviour and Phase Change Material (PCM) transition across the wall assembly, a dynamic heat transfer model was developed using the enthalpy method. This approach handles the moving phase-change interface without requiring explicit tracking of the moving boundary. To formulate the governing transport equations while maintaining computational efficiency, the following simplifying assumptions are made:

- One-dimensional heat transfer (unidirectional);
- Negligible thermal resistance between layers;
- Heat propagation in the wall occurs only by conduction;
- No heat generation is considered;
- The solid body is considered homogeneous;

Temperature profile in x-direction, T(x), is given by the following partial differential equation [35, 36]:

$$\rho c_p \frac{\partial T}{\partial t} = \lambda \frac{\partial^2 T}{\partial x^2} \quad (5)$$

Incorporating volumetric enthalpy into the one-directional transient heat conduction equation yields the following governing equation:

$$\frac{\partial \mathrm{H}(\mathrm{t})}{\partial \mathrm{t}} = \lambda \frac{\partial^2 \mathrm{T}}{\partial \mathrm{x}^2} \quad (6)$$

Where $H$ denotes the total volumetric enthalpy expressed in $(\frac{\mathrm{J}}{m^3})$ and λ is the thermal conductivity of the material in (W/m.K).

Knowing the enthalpy at a given time step [37, 38], the corresponding temperature is determined using the following enthalpy-temperature relationship:

$$T = \frac{H}{C \times \rho} \quad (7)$$

*D. Discretization*

The schematic in Figure 3 depicts the discretization and applied boundary conditions for the multi-layer wall. The transient governing transport equations were solved numerically using an explicit finite-difference method scheme. The domain spatial step $\Delta x$ and computational time step $\Delta t$ are defined as follows:

$$\Delta x = L \times N_x - 1 \quad (8)$$

$$\Delta t = t_{max} \times N_t \quad (9)$$

Where $L$ represents the total wall thickness, $N_x$ is the total number of spatial grid nodes, $t_{max}$ denotes the total simulation period, and $N_t$ is the total number of temporal increments.

The considered wall of N layers was discretized into a number of nodes and the equations were derived by applying the overall energy balance [39, 40], with $\Delta x1 = \Delta x2 = \Delta x$ :

$$\frac{\partial^2 T}{\partial x^2} = \frac{T_{i+1} - 2T_i + T_{i-1}}{\Delta x^2} \quad (10)$$

$$H_i^{n+1} = H_i^n + \frac{\lambda \Delta \mathrm{t}}{\Delta \mathrm{x}^2}\left(T_{i+1}^n - 2T_i^n + T_{i-1}^n\right) \quad (11)$$

For both boundary conditions (inside and outside nodes), the application of the boundary conditions leads to the following two relations:

$$H_0^{k+1} = H_0^k + \left(\frac{\lambda_1 \Delta t}{\Delta x^2}\right) T_1^k - \left(\frac{2\lambda_1 \Delta t}{\Delta x^2} + \frac{2h_{c1}\Delta t}{\Delta x} + \frac{2h_{r,o}\Delta t}{\Delta x}\right) T_0^k + \left(\frac{2\Delta t}{\Delta x}\right)\left(h_{c,1}T_0 + h_{r,o}T_{sky} + \alpha I\right) \quad (12)$$

$$H_n^{k+1} = H_n^k + \left(\frac{\lambda_1 \Delta t}{\Delta x^2}\right) T_{n-1}^k - \left(\frac{2\lambda_1 \Delta t}{\Delta x^2} + \frac{2h_{c2}\Delta t}{\Delta x} + \frac{2h_{r,o}\Delta t}{\Delta x}\right) T_n^k + \left(\frac{2\Delta t}{\Delta x}\right)\left(h_{c,2}T_i\right) \quad (13)$$

Inside the Phase Change Material (PCM) domain, tracking temperature alone is insufficient to describe the thermodynamic state during phase transformation. To overcome this limitation, the enthalpy method is employed, where $H$ represents the total amount of thermal energy per unit volume.

- In the PCM domain, the spatial discretization scheme applied to the PCM layer remains identical to that of the solid brick region, with the governing equations modified to incorporate the phase change effect.
- For an isothermal phase change, the melt PCM mass fraction $f$ is expressed as a function of the local enthalpy as follows :

$$f = \max\left\{\begin{array}{c} 0 \\ \min\left(1, \dfrac{H_i - H_{melt}}{H_{liquid} - H_{melt}}\right) \end{array}\right\} \quad (14)$$

$$f\left\{\begin{array}{ll} 0 \to T < T_f & solid \\ 0\,to\,1 \to T = T_f & Mix \\ 1 \to T > T_f & liquid \end{array}\right\} \quad (15)$$

$$f_i = \frac{H_i - H_{melt}}{H_{liquid} - H_{melt}} \quad (16)$$

- The thermophysical properties of the PCM as a function of liquid fraction are given as:

$$\lambda_i = (1 - f_i)\lambda_s + f_i\lambda_l \quad (17)$$

$$\rho_i = (1 - f_i)\rho_s + f_i\rho_l \quad (18)$$

$$C_i = (1 - f_i)C_s + f_iC_l \quad (19)$$

The temperature in PCM region is calculated as follows:

- Before melting

$$T = T_f + \frac{H}{\rho_s C_s} \quad (20)$$

- After melting

$$T = T_f + \frac{H - \rho_i L_f}{\rho_l C_l} \quad (21)$$

- During melting

Enthalpy-temperature relationship:

- Solid state

$$H_s = \rho_s \cdot C_s\left(T - T_f\right) \quad (22)$$

- Liquid state

$$H_l = \rho_l \cdot C_l\left(T - T_f\right) + \rho_l \cdot L_f \quad (23)$$

Finally, the corresponding sensible volumetric enthalpy is calculated using the following relationship:

$$H_i^{k+1} = H_i^k + \frac{\lambda_{i-1}^k \Delta t}{\Delta x^2} T_{i-1}^k - \frac{\Delta t}{\Delta x^2}\left(\lambda_{i-1}^k + \lambda_{i+1}^k\right)T_i^k + \frac{\lambda_{i+1}^k \Delta t}{\Delta x^2} T_{i+1}^k \quad (24)$$

For an interface node that lies between the two layers (Brick and PCM), it is expressed as:

$$H_i^{k+1} = H_i^k + \left(\frac{\lambda_p \Delta t}{\Delta x^2}\right)T_{i-1}^k - \left(\frac{\Delta t}{\Delta x^2}\right)\left(\lambda_p + \lambda_B\right)T_i^k + \left(\frac{\lambda_B \Delta t}{\Delta x^2}\right)T_{i+1}^k \quad (25)$$

The calculation process initiates with the definition of physical and geometric data, material thermophysical properties, meshing parameters. Then, it initializes the enthalpy distribution across layers. Next, boundary conditions (indoor and outdoor temperatures, convection coefficients) are then defined. The simulation dynamically updates the thermophysical properties, including the calculation of the melted fraction in the PCM zone, which allows the evaluation of the material's effective properties. At each time step, the temperature is recalculated from the enthalpy, which is itself updated using an explicit scheme. Radiative heat transfer is also accounted through the calculation of the radiation coefficient. Finally, internal and external heat fluxes are evaluated, and the results are visualized in the form of temperature profiles and flux graphs. The entire process is represented in the flowchart shown in Figure 4.

The following data have been considered:

- The initial temperature distribution is taken uniform across the whole wall (25 °C), corresponding to the indoor air temperature.
- The same day is repeated until the periodic regime is reached (Section IV.A). The wall without PCM is 0.30 m thick; with the 0.05 m PCM layer the total thickness is 0.35 m.
- The convective heat transfer coefficients at the outdoor and indoor sides are taken as 10 W/m²·K and 8 W/m²·K, respectively; the radiative exchange of the outer surface with the sky is computed with equations (2) and (3).
- The ambient air temperature and the solar radiation on each surface are the hourly values of a typical sunny day and of a heat-wave day of each climatic zone, taken from PVGIS [41] (Section IV.A); the typical days are shown in Fig. 5.
- The absorptivity and the emissivity of the outer surface are 0.6 and 0.85, and the indoor air temperature is 25 °C.
- The initial temperature of the wall is 25 °C and has no effect on the periodic regime. For

PCMs given with a melting range, the phase change is taken as isothermal at the mean value of the range.

*E. Performance indicators*

In addition to the temperature profiles, four indicators are taken from the last day of each simulation: the maximum internal surface temperature, the daily amplitude of the internal surface temperature (maximum minus minimum), the maximum heat flux at the internal surface, and the daily heat gain through the internal surface (heat flux integrated over 24 h). The heat flux is $q_i = h_{c,i} (T_{s,i} - T_i)$, where $T_{s,i} = T_{x=L}$ is the internal surface temperature (Eq. (4)), $T_i$ is the indoor air temperature and $h_{c,i}$ is the indoor convective coefficient; $q_i$ is positive towards the room. The reduction of the daily heat gain is given relative to the wall without PCM.

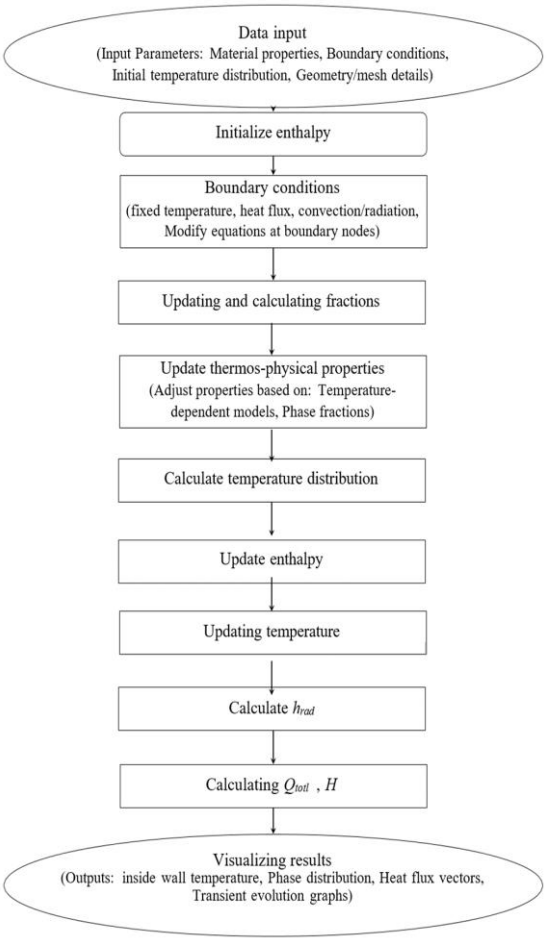



**Fig 4. Computational procedure flowchart.**

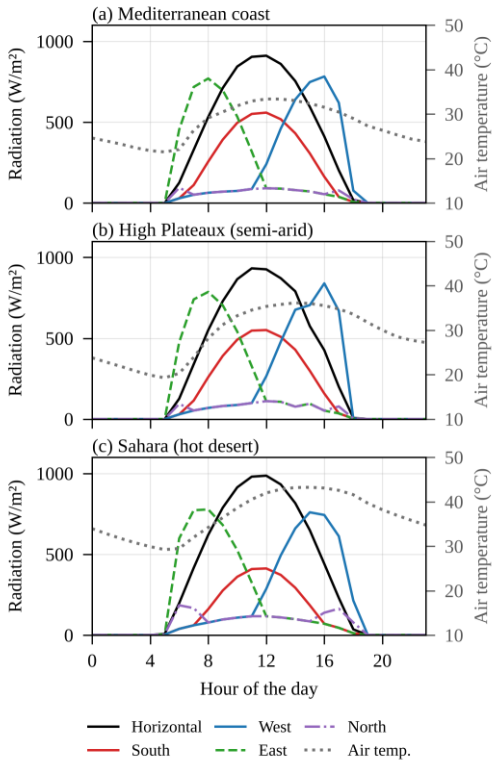



**Fig 5. Hourly solar radiation on the five surfaces (continuous, dashed and dash-dotted lines) and air temperature (dotted line) of the typical sunny day of the three climatic zones: (a) Mediterranean coast, (b) High Plateau, (c) Sahara.**

*F. Numerical parameters and verification*

The explicit scheme is stable only if the time step is below a limit, which is 6.6 s with Δx = 2.5 mm (set by the brick nodes). A mesh of N = 141 nodes and Δt = 3 s, about half of this limit, was used for the 0.35 m wall. Taking Δx = 1.25 mm and Δt = 0.75 s as reference for RT-27 between the bricks, the maximum internal surface temperature changes by 0.001 °C, the maximum heat flux by 0.008 W/m² and the daily heat gain by 0.17 %; the energy balance is closed to machine precision (relative error below 1e-12 %). The phase-change treatment was verified against the analytical (Neumann) solution of the Stefan problem: melting of a 0.4 m slab of RT-27, initially at 25 °C, with the surface kept at 45 °C. After 6 h the melting front is at 31.3 mm in the analytical solution and the numerical value differs by 0.18 %; the maximum temperature deviation is 0.10 °C and the rms deviation is 0.019 °C (Fig. 6).

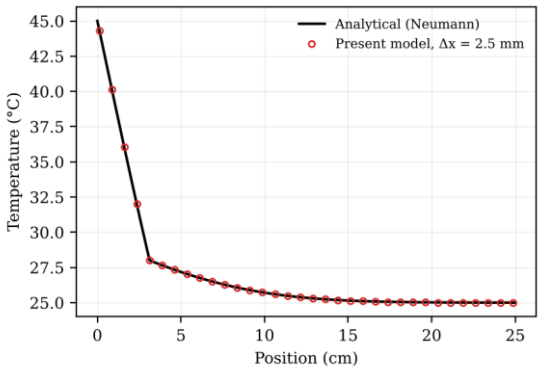



**Fig 6. Verification of the study model against the analytical solution of the Stefan problem after 6 h (RT-27, surface at 45 °C).**

## IV. APPLICATION TO THREE CLIMATIC ZONES OF ALGERIA

### *A. Climatic zones, data and simulation cases*

The general approach of Sections I to III is applied to three climatic zones of Algeria, with one site per zone, a typical sunny day and a heat-wave day for each site, and the five surfaces (roof and four walls). The wall without PCM is analysed first (Section V.A), then RT-27 is studied for the three positions and the five orientations (Sections V.B and V.C), three PCMs are compared (Section V.D), and the melting temperature is varied (Section V.E).

The simulations are made in a periodic regime: the daily profile of outdoor temperature and solar radiation is repeated until the maximum internal surface temperature of two consecutive days differs by less than 0.005 °C, the last day is analysed, and the indoor air is at 25 °C. The same model ($\Delta x = 2.5$ mm, $\Delta t = 3$ s) was applied to one representative site per climatic zone: the Mediterranean coast (hot-summer Mediterranean climate, Köppen Csa; 36.76° N, 2.95° E), the High Plateau (semi-arid, BSk; 34.68° N, 3.25° E) and the Sahara (hot desert, BWh; 31.96° N, 5.36° E), with hourly PVGIS data of 2023 (ERA5-Land air temperature, 9 km grid) [41]. The radiation on the five surfaces (horizontal, and vertical walls facing south, west, east and north) was taken directly from PVGIS for fixed planes, so no transposition model was needed. A typical sunny day and a heat-wave day were selected for each site with the same rule. The melting temperature was varied from 18 to 44 °C with the other properties of RT-27, and each case was compared with the same layer without latent heat. The typical day reaches 33, 36 and 43 °C in the three zones (Fig. 5), with a peak global horizontal radiation of 911, 932 and 986 W/m², and the heat-wave day 45, 39 and 49 °C: the zones differ mainly by the air temperature.

## V. RESULTS AND DISCUSSION

All the results are given for the periodic regime (Section IV.A): the last day of the simulation is analysed, for a typical sunny day and a heat-wave day of each zone and for the five surfaces. The wall without PCM is the reference, and the PCM is RT-27 unless stated otherwise. The numerical values are collected in Tables 3 to 10, and the text analyses their variation.

### *A. Temperature in the wall and effect of the PCM layer (objective 1)*

Table 3 gives the daily minimum, mean and maximum temperature at the three positions of the layer in the wall without PCM. The exterior position follows the outdoor air and the solar load (Fig. 7) and has the widest range, the interior position stays close to the indoor air temperature, and the position between the bricks is in between, with a delay of several hours. The mean temperature increases from the interior to the exterior position, towards the Sahara and on the heat-wave day.

*Table 3*

Daily minimum / mean / maximum temperature (°C) at the three positions of the layer in the wall without PCM (mean of the five surfaces)

| Position | Coast, typical | Coast, heat wave | High Plateau, typical | High Plateau, heat wave | Sahara, typical | Sahara, heat wave |
|---|---|---|---|---|---|---|
| Exterior | 21 / 29 / 40 | 26 / 35 / 47 | 20 / 30 / 42 | 24 / 33 / 44 | 29 / 38 / 48 | 32 / 41 / 53 |
| Between bricks | 25 / 27 / 30 | 28 / 31 / 34 | 25 / 28 / 31 | 27 / 30 / 32 | 30 / 33 / 35 | 32 / 35 / 37 |
| Interior | 25 / 26 / 27 | 27 / 28 / 29 | 25 / 27 / 28 | 26 / 28 / 29 | 28 / 29 / 30 | 29 / 30 / 31 |

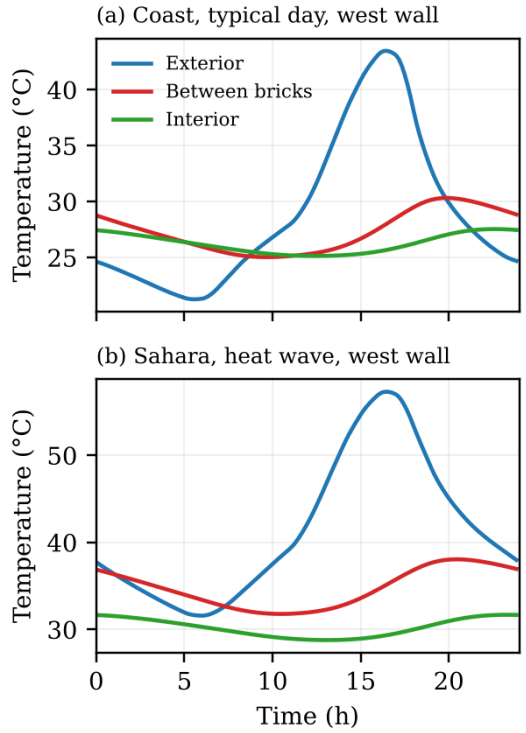



**Fig 7. Temperature at the three positions of the layer in the wall without PCM (west wall): (a) coast, typical day; (b) Sahara, heat-wave day.**

The PCM layer lowers the maximum internal surface temperature and flattens its daily variation (Fig. 8). With RT-27 the reduction is about 1 to 2 °C on average over the five surfaces (Table 4); it is larger on the heat-wave day and in the Sahara, and the daily heat gain through the internal surface falls by about 30 % in all the cases.

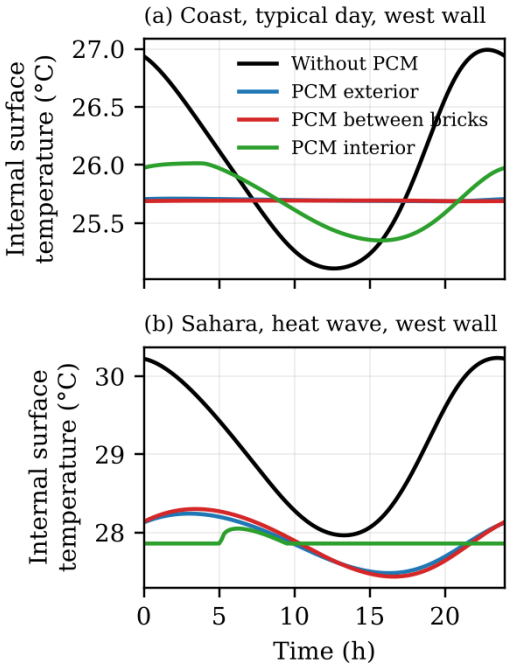



**Fig 8. Internal surface temperature of the west wall without PCM and with RT-27 at the three positions: (a) coast, typical day; (b) Sahara, heat-wave day.**

*B. Influence of the PCM position (objective 2)*

Table 4 compares the three positions of the layer. With RT-27, the interior position gives on average the largest reduction, and the exterior and between-bricks positions almost the same one. The reason is that the melting temperature of RT-27 (28 °C) is close to the mean daily temperature of the interior position (Table 3), but much lower than that of the exterior position, where the PCM stays liquid during a large part of the day. At the optimum melting temperature of each position (last three columns of Table 4) the three positions give the same reduction, so the position matters less than the melting temperature. This explains why the best position differs in the literature (exterior in [7, 8], interior or middle in [9, 10]): it is the one where the mean daily temperature is close to the melting temperature of the PCM, so it depends on the climate [11, 12], on the wall and on the PCM.

*Table 4*

Maximum internal surface temperature without PCM (°C) and its reduction (°C) with RT-27 and with the optimum melting temperature Tm* at the exterior, between-bricks and interior positions (mean of the five surfaces)

| Zone, day | No PCM | RT-27 ext. | RT-27 betw. | RT-27 int. | Tm* ext. | Tm* betw. | Tm* int. |
|---|---|---|---|---|---|---|---|
| Coast, typical | 26.9 | 1.08 | 1.05 | 0.95 | 1.15 | 1.17 | 1.14 |
| Coast, heat wave | 28.4 | 1.42 | 1.39 | 1.65 | 1.68 | 1.68 | 1.68 |
| High Plateau, typical | 27.2 | 1.15 | 1.17 | 1.20 | 1.30 | 1.31 | 1.27 |

| | | | | | | | |
|---|---|---|---|---|---|---|---|
| High Plateau, heat wave | 27.9 | 1.23 | 1.21 | 1.38 | 1.43 | 1.43 | 1.43 |
| Sahara, typical | 29.0 | 1.50 | 1.45 | 1.60 | 1.75 | 1.74 | 1.75 |
| Sahara, heat wave | 30.0 | 1.82 | 1.77 | 1.95 | 2.09 | 2.08 | 2.10 |

*C. Influence of the wall orientation (objective 2)*

Without PCM, the maximum internal surface temperature depends strongly on the orientation (Table 5): the roof is the hottest, the east, south and west walls come next, and the north wall is the coolest, with a range of about 3 °C in all the cases. With RT-27 between the bricks the temperatures fall and the range falls to 1.7 to 2.0 °C (Fig. 9). The gain brought by the PCM is the largest on the roof, where the solar load is the largest, and the smallest on the north wall, but the PCM does not make the indoor surface independent of the facade; part of this levelling comes from the added layer itself (Section V.E). PCM panels are therefore most useful on roofs and on west and south walls.

*Table 5*

Maximum internal surface temperature (°C) without PCM / with RT-27 between the bricks, by orientation

| Surface | Coast, typical | Coast, heat wave | High Plateau, typical | High Plateau, heat wave | Sahara, typical | Sahara, heat wave |
|---|---|---|---|---|---|---|
| Roof | 28.4 / 26.8 | 30.1 / 28.1 | 28.8 / 27.2 | 29.6 / 27.8 | 30.7 / 28.6 | 31.7 / 29.3 |
| South wall | 26.8 / 25.7 | 27.9 / 26.7 | 27.2 / 25.9 | 27.4 / 26.3 | 28.4 / 27.2 | 29.4 / 27.8 |
| East wall | 26.7 / 25.7 | 28.2 / 27.0 | 27.0 / 25.9 | 27.7 / 26.7 | 28.8 / 27.5 | 29.7 / 28.1 |
| West wall | 27.0 / 25.7 | 28.6 / 27.1 | 27.4 / 25.9 | 27.9 / 26.7 | 29.3 / 27.6 | 30.2 / 28.3 |
| North wall | 25.4 / 25.2 | 27.2 / 26.1 | 25.9 / 25.4 | 26.7 / 25.8 | 27.8 / 26.8 | 28.9 / 27.5 |
| Range | 3.0 / 1.7 | 3.0 / 2.0 | 2.9 / 1.7 | 2.9 / 2.0 | 2.9 / 1.7 | 2.8 / 1.7 |

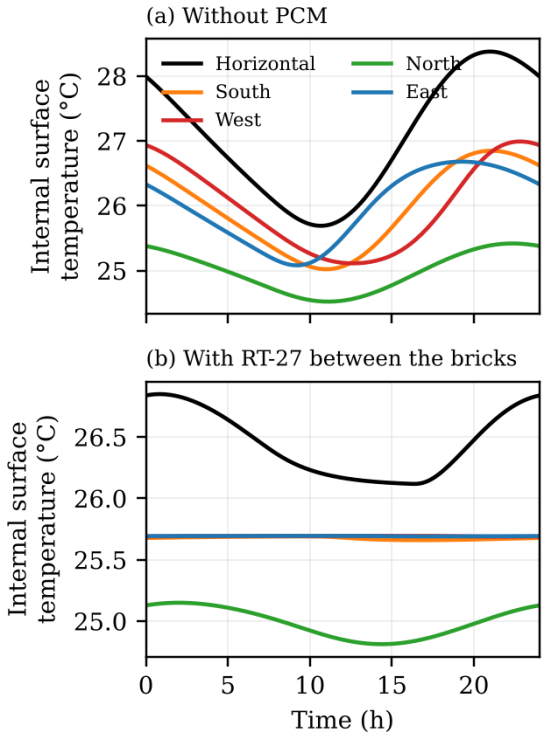



**Fig 9. Internal surface temperature for the five orientations on the coast, typical day: (a) without PCM, (b) with RT-27 between the bricks.**

*D. Influence of the PCM type (objective 3)*

Eight commercial PCMs with melting temperatures from 5 to 29 °C were first considered. Those melting at 5 to 24 °C (RT-23, PX-15, RT-5, S19 and HS-21) are below nearly all the temperatures reached at the layer (Table 3), so they stay liquid, cannot store latent heat and act only as sensible storage; they are not studied. Three PCMs remain (Table 6): RT-27, n-octadecane and $CaCl_2 \cdot 6H_2O$, with melting temperatures of 28 to 29 °C.

*Table 6*

Thermophysical properties of the three PCMs studied

| PCM | Name | Class | Type | Melting temperature Tm (°C) | Specific heat capacity | Volumetric mass density | Latent heat of fusion | Thermal conductivity |
|---|---|---|---|---|---|---|---|---|

| | | | | | C ( $\frac{J}{kg \cdot K}$ ) | ρ ( $\frac{kg}{m^3}$ ) | Lf ( $\frac{kJ}{kg}$ ) | λ ( $\frac{W}{m.K}$ ) |
|---|---|---|---|---|---|---|---|---|
| PCM1 | RT-27 | Organic | Paraffin | 28 | 2000 | 870 | 147 | 0.20 |
| PCM2 | n-Octadecane | Organic | Pure paraffin | 28 | 2400 | 814 | 245 | 0.358 |
| PCM3 | $CaCl_2 \cdot 6H_2O$ | Inorganic | Pure salt hydrate | 29 | 3020 | 1700 | 190 | 1.00 |

Table 7 and Fig. 10 show that RT-27 gives the largest reduction in the three zones, followed by n-octadecane and $CaCl_2 \cdot 6H_2O$, and that the reduction is the largest in the Sahara for the three PCMs. The latent heat contributes little for the three of them, because their melting temperature is not the optimum of the position (Section V.E). RT-27 and n-octadecane both melt at 28 °C and RT-27 gives the larger reduction, probably because of its lower conductivity (0.2 against 0.358 W/m·K); $CaCl_2 \cdot 6H_2O$, with a conductivity of 1.0 W/m·K, is the least effective. In agreement with [18, 19], only the PCMs whose melting temperature is within the range reached in the wall can use their latent heat.

*Table 7*

Reduction of the maximum internal surface temperature (°C) by the three PCMs between the bricks (median over the surfaces and the two days), share of the latent heat in it and reduction of the daily heat gain (median)

| PCM | Coast | High Plateau | Sahara | Latent heat share (%) | Heat gain reduction (%) |
|---|---|---|---|---|---|
| RT-27 | 1.22 | 1.18 | 1.59 | 5 | 29 |
| n-Octadecane | 0.96 | 0.95 | 1.16 | 3 | 19 |
| $CaCl_2 \cdot 6H_2O$ | 0.69 | 0.71 | 0.83 | 0 | 8 |

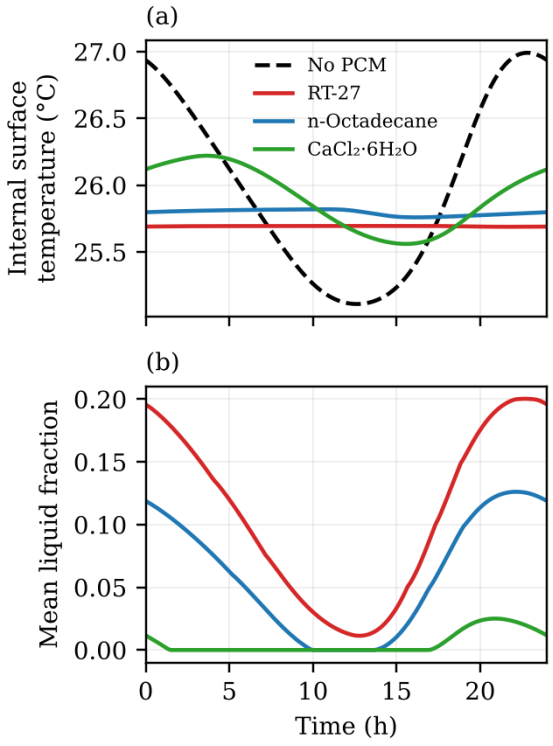



**Fig 10. Internal surface temperature (a) and mean liquid fraction (b) of the three PCMs between the bricks (west wall, coast, typical day).**

*E. Latent heat, periodic regime and optimum melting temperature (objective 4)*

To separate the latent heat from the effect of the added layer, each PCM was also simulated with zero latent heat. With RT-27 at 28 °C the latent heat is a median of 5 % of the reduction (Table 7), because 28 °C is not the right melting temperature in most cases. When the melting temperature is optimised, the latent heat lowers the maximum internal surface temperature by 0.1 to 0.5 °C (median 0.3 °C) relative to the same layer without latent heat, whereas the layer lowers it by 0.3 to 2.5 °C (median 1.2 °C) relative to the wall without PCM; the PCM layer at its optimum melting temperature lowers it by 0.4 to 2.9 °C (median 1.5 °C) in total, and the latent heat is a median of 20 % of it. The reduction depends on the melting temperature as shown in Fig. 11: the curve is flat, equal to the layer without latent heat, when the PCM is always liquid or always solid, and has a minimum when the melting temperature lies within the range reached at the position of the layer.

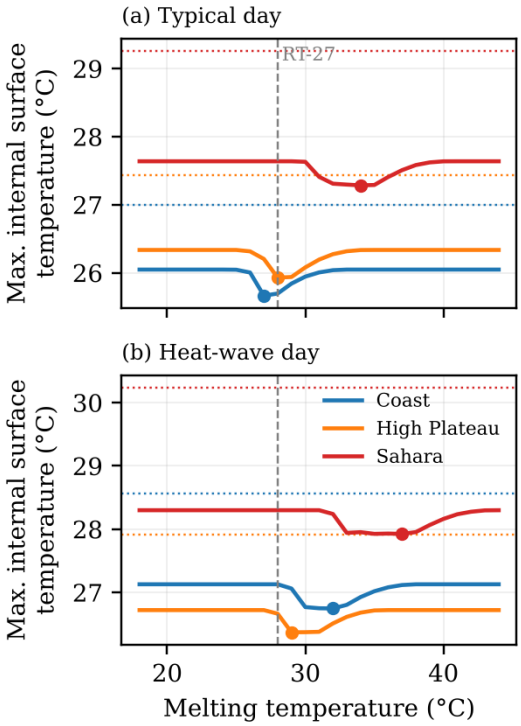



**Fig 11. Maximum internal surface temperature as a function of the melting temperature of the layer between the bricks (west wall): (a) typical day; (b) heat-wave day. Points: optimum; dotted lines: wall without PCM; dashed line: RT-27.**

Table 8 gives, for each position and each surface, the optimum melting temperature Tm* of Eq. (T7). It increases from the interior to the exterior position, from the walls to the roof and from the coast to the Sahara, and by 1.8 to 3.5 °C from the typical to the heat-wave day between the bricks; among the walls, the north wall has the lowest value and the east and west walls the highest. RT-27 (28 °C) is close to the optimum only at the interior side, and between the bricks in the Sahara it stays liquid all day. The optimum varies little with ±10 % of solar load (1.0 °C at most) but rises by 2.0 to 5.0 °C when the indoor air goes from 25 to 31 °C, so Table 8 applies to air-conditioned buildings.

The optimum is close to the mean daily temperature at the position of the layer in the wall without PCM (Table 3), which is the usual criterion for selecting a PCM [42]. Table 9 shows that choosing Tm equal to this mean temperature gives a mean excess of the maximum internal surface temperature over its minimum of 0.07 °C, against 0.04 °C for the optimum Tm* and 0.19 °C for RT-27; the correlation between the two temperatures is 0.97, and they differ by 1 °C or more in 17 of the 42 cases (up to 2.6 °C, exterior position).

The mean daily temperature of the wall without PCM is therefore a good first choice, refined by Table 8.

Table 8 could serve as a starting point for comparable climates (for instance in North Africa), but it depends on the daily temperature and on the indoor air temperature, and no site outside Algeria was simulated.

*Table 8*

Optimum melting temperature Tm* (°C) by position and surface (periodic regime, 25 °C indoors)

| Position, surface | Coast (Alger) | High Plateau (Djelfa) | Sahara (Ouargla) |
|---|---|---|---|
| Between bricks, roof | 32 | 32 | 38 |
| Between bricks, south wall | 29 | 29 | 33 |
| Between bricks, east wall | 30 | 29 | 34 |
| Between bricks, west wall | 30 | 29 | 35 |
| Between bricks, north wall | 28 | 28 | 32 |
| Interior, roof | 29 | 30 | 32 |
| Interior, south wall | 27 | 27 | 30 |
| Interior, east wall | 27 | 27 | 30 |
| Interior, west wall | 27 | 27 | 31 |
| Interior, north wall | 28 | 25* | 29 |
| Exterior, roof | 37 | 35 | 42 |
| Exterior, south wall | 32 | 30 | 36 |
| Exterior, east wall | 33 | 32 | 38 |
| Exterior, west wall | 33 | 31 | 38 |
| Exterior, north wall | 30 | 26 | 35 |

* The optimum, 25 °C, only holds the surface at the indoor air temperature.

.

*Table 9*

Mean daily temperature T at the position of the layer in the wall without PCM, optimum melting temperature Tm*, and mean excess of the maximum internal surface temperature over its minimum with Tm = T and with RT-27 (mean of the surfaces)

| Position, zone | Mean T (°C) | Tm* (°C) | Excess with T (°C) | Excess with RT-27 (°C) |
|---|---|---|---|---|
| Between bricks, Coast | 29.0 | 29.8 | 0.16 | 0.21 |
| Between bricks, High Plateau | 29.0 | 29.4 | 0.05 | 0.18 |
| Between bricks, Sahara | 33.6 | 34.4 | 0.01 | 0.30 |
| Interior, Coast | 27.5 | 27.5 | 0.02 | 0.14 |
| Interior, High Plateau | 27.4 | 27.8 | 0.02 | 0.05 |
| Interior, Sahara | 29.9 | 30.8 | 0.07 | 0.18 |
| Exterior, Coast | 31.9 | 33.0 | 0.12 | 0.17 |
| Exterior, High Plateau | 31.8 | 30.8 | 0.07 | 0.18 |
| Exterior, Sahara | 39.6 | 37.8 | 0.06 | 0.26 |
| All cases | 31.3 | 31.4 | 0.07 | 0.19 |

As the latent heat is small, the layer thickness should be studied together with Tm.

Comparison with conventional insulation. The 0.05 m PCM layer between the bricks was replaced by 0.05 m of expanded polystyrene ($\rho$ = 30 kg/m³, c = 1400 J/kg·K, $\lambda$ = 0.036 W/m·K) for the roof and the west wall of the three zones, on the typical and heat-wave days (Table 10). The insulation lowers the maximum internal surface temperature and the daily heat gain more than the PCM, even at its optimum melting temperature. On thermal grounds alone, a PCM layer therefore does not replace insulation here, and the latent heat cannot justify it alone; its interest would come from its combination with insulation [22], from effects not studied here (peak shift, winter) or from its cost, which was not assessed.

*Table 10*

Insulation compared with the PCM layer between the bricks: median (minimum – maximum) over the roof and the west wall of the three zones, typical and heat-wave days

| Solution | Reduction of max. Ts,i (°C) | Reduction of daily heat gain (%) |
|---|---|---|
| 0.05 m expanded polystyrene | 3.0 (1.6 – 4.9) | 70 |
| PCM at its optimum Tm* | 2.0 (1.3 – 2.9) | 29 |
| RT-27 (28 °C) | 1.6 (1.3 – 2.4) | 29 |

Limitations and future work. The model is one-dimensional and considers conduction only; the thermal resistance between layers is neglected, the phase change is isothermal at the mean value of the melting range (no hysteresis), natural convection in the melted PCM is not included, and the density is constant. The properties of RT-27 are manufacturer values and vary between sources (Section II); with an earlier set (melting range 28–30 °C, Lf = 179 kJ/kg, c = 2400 J/kg·K, $\lambda$ = 0.23 W/m·K) the maximum internal surface temperature differed by 0.3 °C at most, but the optimum melting temperature of the heat-wave day (roof and west wall between the bricks) by up to 4 °C, so Table 8 depends on the properties assumed. The simulations use one typical and one heat-wave day per zone, 2023 PVGIS data for one site per zone, assumed absorptivity and emissivity, an indoor air at 25 °C and a PCM thickness of 0.05 m; cost and durability are not considered. No experimental validation was done; the model was verified numerically (Section III.F). These points limit the absolute values, not the comparison between cases. The next steps are an experimental validation on a test cell, the coupling with a free-floating indoor temperature, and the study of the thickness and of the economic feasibility of the PCM layer, alone or combined with insulation.

## CONCLUSION

In this study, the heat transfer through a multilayer brick wall with a PCM layer was modelled with the enthalpy method in a periodic regime, and the

PCM position, the wall orientation and the PCM type were analysed in one framework for three climatic zones of Algeria (Mediterranean coast, semi-arid High Plateau and hot desert), on a typical sunny day and a heat-wave day.

The model was verified against the analytical solution of the Stefan problem. The main findings are:

- With RT-27, the maximum internal surface temperature falls by 1 to 2 °C on average over the five surfaces (up to 2.5 °C for the roof) and the daily heat gain by about 30 % (Table 4); the effect is larger on the heat-wave day and in the Sahara.
- The position of the layer matters less than its melting temperature: with RT-27 the interior position is slightly better, and at the optimum melting temperature of each position the three positions give the same reduction.
- The orientation changes the maximum internal surface temperature by about 3 °C without PCM and by about 1.7 to 2.0 °C with PCM, so the PCM is most useful on the roof and on west and south walls.
- Among the three PCMs whose melting temperature is reached in the wall, RT-27 gives the largest reduction, followed by n-octadecane and $CaCl_2 \cdot 6H_2O$; PCMs melting below the temperatures of the wall act only as sensible storage.
- At the optimum melting temperature, the PCM lowers the maximum internal surface temperature by 0.4 to 2.9 °C (median 1.5 °C), but the latent heat adds only 0.1 to 0.5 °C (median 20 % of the reduction): most of the benefit comes from the added layer.
- The optimum melting temperature increases from the interior to the exterior position, from the walls to the roof and from the coast to the Sahara. Between the bricks it is 28 to 30 °C for the walls and 32 °C for the roof on the coast and the High Plateau, and 32 to 35 °C and 38 °C in the Sahara. It is close to the mean daily temperature at the position of the layer, which can be used to select the PCM.
- 0.05 m of expanded polystyrene lowers the maximum internal surface temperature more than the PCM (median 3.0 °C against 2.0 °C at the optimum melting temperature) and the daily heat gain by 70 % against 30 %.
- Final position. For the brick exterior wall studied here, in the Algerian climates considered, a PCM layer is not an effective stand-alone solution: its benefit is modest (1 to 2 °C), comes mostly from the added layer, and is smaller than that of the same thickness of thermal insulation. A PCM is worth considering only together with insulation, on roofs and on west and south walls, and with a melting temperature chosen from the mean daily temperature of the wall at the position of the layer (28 to 30 °C for walls and 32 °C for roofs on the coast and the High Plateau, 32 to 38 °C in the Sahara) instead of a standard value such as RT-27; this combination and its economic justification remain to be assessed.

These results give criteria for the selection and placement of PCM wall panels in buildings of comparable climates. Experimental validation and an economic assessment, alone or combined with insulation, are the next steps.

## REFERENCES

[1] Laidi, S., El Hassar, S.M.K., Mahrane, A., Sellami, R., Study and modeling of the thermal behavior of buildings with attic roof in the Algerian climate context. *International Journal of Sustainable Building Technology and Urban Development*, 2024, vol. 15, no. 1, pp. 3-22.

[2] Rashid, F.L., Al-Obaidi, M.A., Dulaimi, A., Mahmood, D.M., Sopian, K., A review of recent improvements, developments, and effects of using phase-change materials in buildings to store thermal energy. *Designs*, 2023, vol. 7, no. 4, pp. 90.

[3] Pomianowski, M., Heiselberg, P., Zhang, Y., Review of thermal energy storage technologies based on PCM application in buildings. *Energy and Buildings*, 2013, vol. 67, pp. 56-69.

[4] Gobinath, S., Senthilkumar, G., Beemkumar, N., Comparative study of room temperature control in buildings with and without the use of PCM in walls. Energy Sources, Part A: Recovery, *Utilization, and Environmental Effects*, 2018, vol. 40, no. 14, pp. 1765-1771.

[5] Anter, A.G., Sultan, A.A., Hegazi, A.A., El Bouz, M. A., Thermal performance and energy saving using phase change materials (PCM) integrated in building walls. *Journal of Energy Storage*, 2023, vol. 67, pp. 107568.

[6] Caggiano, A., Mankel, C., Koenders, E. Reviewing theoretical and numerical models for PCM-embedded cementitious composites. *Buildings*, 2018, vol. 9, no. 1, pp. 3.

[7] Khan, R.J., Bhuiyan, M.Z.H., Ahmed, D.H., Investigation of heat transfer of a building wall in the presence of phase change material (PCM). *Energy Built Environ*, 2020, vol. 1, no. 2, pp 199–206.

[8] Lajimi, N., Boukadida, N., Effect of the position of the PCM on the thermal behavior of a multilayer wall of a building in summer period. *Frontiers in Environmental Science*, 2023, vol. 11, art. 1226454.

[9] Nateghi, S.K., Jahangir, M.H. Evaluation of phase change material's location in the wall building in thermal energy storage, 2020, *28th Annual International Conference of Iranian Society of Mechanical Engineers*.

[10] Liu, S., Wang, J., Meng, L., Hu, C., Meng, X., Location of the phase-change material layer on thermal performance of light-weight walls. *International Journal of Low-Carbon Technologies*, 2024, vol. 19, pp. 127-134.

[11] Kishore, R.A., Bianchi, M.V., Booten, C., Vidal, J., Jackson, R. Optimizing PCM-integrated walls for potential energy savings in US Buildings. *Energy and Buildings*, 2020, vol. 226, art. 110355.

[12] Zhu, N., Li, S., Hu, P., Lei, F., Deng, R. Numerical investigations on performance of phase change material Trombe wall in building. *Energy*, 2019, vol. 187, art. 116057.

[13] Arici, M., Bilgin, F., Nižetić, S., Karabay, H., PCM integrated to external building walls: An optimization study on maximum activation of latent heat. *Applied Thermal Engineering*, 2020, vol. 165, art. 114560.

[14] de Gracia, A., Dynamic building envelope with PCM for cooling purposes–Proof of concept. *Applied energy*, 2019, vol. 235, pp. 1245-1253.

[15] Salihi, M., El Fiti, M., Harmen, Y., Chhiti, Y., Chebak, A., Alaoui, F. E. M. H., Jama, C., Evaluation of global energy performance of building walls integrating PCM: Numerical study in semi-arid climate in Morocco. *Case Studies in Construction Materials*, 2022, vol. 16, art. 00979.

[16] Alwan, M. S., Jalghaf, H. K., Long Term Heat Transfer Simulation Through multilayer building wells with Phase Change Materials. *Al-Iraqia Journal for Scientific Engineering Research*, 2024, vol. 3, no. 3, pp. 80-93.

[17] M'ziane, M. C., Grine, A., Younsi, Z., Touhami, M. S. K., Modelling and numerical simulation of a passive wall incorporating a phase change material. J. Adv. Res. Fluid Mech. *Therm. Sci*, 2021, vol. 79, pp. 169-181.

[18] Dashtaki, A.S., Nadooshan, A.A., Abedi, A., The Effect of Type and Location of a Phase Change Material (PCM) Layer in a Building Wall on Energy Consumption using Numerical Simulation. *International Journal of Advanced Design & Manufacturing Technology*, 2019, vol. 12, no. 4.

[19] Guermat, Z., Kabar, Y., Kuznik, F., Boukelia, T. E., Numerical investigation of the integration of new bio-based PCM in building envelopes during the summer in Algerian cities. *Journal of Energy Storage*, 2024, vol. 79, art. 110111.

[20] Sarrafha, H., Kasaeian, A., Jahangir, M. H., Taylor, R. A., Transient thermal response of multi-walled carbon nanotube phase change materials in building walls. *Energy*, 2021, vol. 224, pp. 120120.

[21] Yehya, N., Maatouk, C., Charaf, H., Numerical Analysis of Phase-Change Material Integration in Building Envelopes: A Case Study in Lebanon. *Buildings*, 2025, vol. 15, no. 8, pp. 1369.

[22] Dardouri, S., Mankai, S., Almoneef, M. M., Mbarek, M., Sghaier, J., Energy performance based optimization of building envelope containing PCM combined with insulation considering various configurations. *Energy Reports*, 2023, vol. 10, pp. 895-909.

[23] Greesan, R., Mekala, C., Rajesh, B., Numerical study and experimental validation of heat transfer in a CenoPCM reinforced multi-layered meta-material wall for energy efficient buildings. *Building services engineering research & technology*, 2024, vol. 45, no. 6, pp. 815-832.

[24] Vedrtnam, A., Kalauni, K., Soares, N., Salazar, B., Ostertag, C. P., Taylor, H. K., Phase change materials for climate-adaptive buildings: A review framed by tropical and Mediterranean climates. *Journal of Energy Storage*, 2025, vol. 125, art.116938.

[25] Lahoud, C., Chahwan, A., Rishmany, J., Yehia, C., Daaboul, M., Enhancing Energy Efficiency in Mediterranean Coastal Buildings Through PCM Integration. *Buildings*, 2024, vol. 14, no. 12, art. 4023.

[26] Li, Z., Du, C., Ahmadi, D., Kalbasi, R., Rostami, S. Numerical modeling of a hybrid PCM-based wall for energy usage reduction in the warmest and coldest months. *Journal of Thermal Analysis & Calorimetry*, 2021, vol. 144, no. 5.

[27] Fathi, A., Badr, O., Soufyane, N., Miriam, M., Youssef, E. M., Brahim, D., Sadoune, Z., Numerical Study on PCM Geometries to enhance Thermal Performance of Building Envelopes. *Journal of Engineering Research*, 2025.

[28] Sarri, A., Bechki, D., Bouguettaia, H., Al-Saadi, S.N., Boughali, S., Farid, M.M. Effect of using PCMs and shading devices on the thermal performance of buildings in different Algerian climates. A simulation-based optimization. *Solar Energy*, 2021, vol. 217, pp. 375-389

[29] Ali-Toudert, F., Weidhaus, J., Numerical assessment and optimization of a low-energy residential building for Mediterranean and Saharan climates using a pilot project in Algeria. *Renewable Energy*, 2017, vol. 101, pp. 327-346.

[30] Biswas, K., Lu, J., Soroushian, P., Shrestha, S. Combined experimental and numerical evaluation of a prototype nano-PCM enhanced wallboard. *Applied energy*, 2014, vol. 131, pp. 517-529.

[31] Al-Yasiri, Q., Szabó, M., Incorporation of phase change materials into building envelope for thermal comfort and energy saving: A comprehensive analysis. *Journal of Building engineering*, 2021, vol. 36, pp. 102122.

[32] Sun, X., Medina, M. A., Lee, K. O., & Jin, X. (2018). Laboratory assessment of residential building walls containing pipe-encapsulated phase change materials for thermal management. Energy, 163, 383-391.

[33] Xu, X., Zhang, Y., Lin, K., Di, H., Yang, R., Modeling and simulation on the thermal performance of shape-stabilized phase change material floor used in passive solar buildings. *Energy and Buildings*, 2005, vol. 37, no. 10, pp.1084-1091.
[34] Zwanzig, S. D., Lian, Y., Brehob, E. G. Numerical simulation of phase change material composite wallboard in a multi-layered building envelope. *Energy Conversion and Management*, 2013, vol. 69, pp.27-40.
[35] Pasupathy, A., Athanasius, L., Velraj, R., Seeniraj, R.V., Experimental investigation and numerical simulation analysis on the thermal performance of a building roof incorporating phase change material (PCM) for thermal management. *Applied Thermal Engineering*, 2008, vol. 28, no. 5-6, pp. 556-565.
[36] Al-Sanea, S. A., Zedan, M. F., Al-Hussain, S. N., Effect of thermal mass on performance of insulated building walls and the concept of energy savings potential. *Applied Energy*, 2012, vol. 89, no. 1, pp.430-442.
[37] Kuznik, F., Virgone, J., Experimental investigation of wallboard containing phase change material: Data for validation of numerical modeling. *Energy and Buildings*, 2009, vol. 41, no. 5, pp.561-570.
[38] Castellón, C., Günther, E., Mehling, H., Hiebler, S., Cabeza, L. F., Determination of the enthalpy of PCM as a function of temperature using a heatflux DSC—A study of different measurement procedures and their accuracy. *International Journal of Energy Research*, 2008, vol. 32, no. 13, pp. 1258-1265.
[39] Jalghaf, H. K., Kovács, E., Simulation of phase change materials in building walls using effective heat capacity model by recent numerical methods. *Journal of Energy Storage*, 2024, vol. 83, art.110669.
[40] Wilson, K., Goldstein, A., Falge, E., Aubinet, M., Baldocchi, D., Berbigier, P., Verma, S. Energy balance closure at FLUXNET sites. *Agricultural and forest meteorology*, 2002, vol. 113, no. 1-4, pp. 223-243.
[41] Huld, T., Müller, R., Gambardella, A. A new solar radiation database for estimating PV performance in Europe and Africa. *Solar Energy*, 2012, vol. 86, no. 6, pp. 1803–1815.
[42] Nizovtsev, M.I., Sterlyagov, A.N. Effect of phase change material (PCM) on the thermal inertia of walls in lightweight buildings. *Journal of Building Engineering*, 2024, vol. 82, art. 107912.

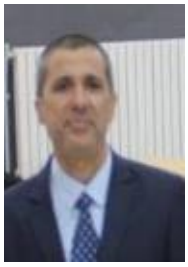
**About Authors.**



**Belkacem Nefissa,**
Assistant Professor at the Department of Common Core in Technology, Faculty of Technology. University Morsli Abdellah of Tipaza. Research interests: Thermal energy systems, PCM, building energy efficiency, solar energy, MATLAB.
*Laboratory of Control, Tests, Measures and Mechanical simulation*.
ORCID: 0000-0002-6734-4380
E-mail: n.belkacem@univ-chlef.dz



**Missoum Mohammed,**
Associate Professor at the Department of mechanical engineering, Faculty of Sciences, University of Tipaza. Research interests: Renewable energy, thermal energy systems, PCM, TRNSYS. *Laboratory of Energy, materials and numerical modeling*. ORCID:0000-0002-8183-8352. E-mail: missoum.mohammed@cu-tipaza.dz



**Benchamma Sofiane,**
Assistant Professor at the Department of mechanical engineering, Faculty of Sciences, University Morsli Abdellah of Tipaza. Research interests: Thermal energy systems, Solar-assisted systems, TRNSYS, PCM.
*Laboratory of Control, Tests, Measures and Mechanical simulation*.
ORCID: 0009-0009-0675-3576. E-mail: s.benchamma@univ-chlef.dz